American Mineralogist, Volume 92, pages 1200–1212, 2007

Mechanisms of diamond oxidation and their bearing on the fluid composition in kimberlite magmas

YANA FEDORTCHOUK,[1] DANTE CANIL,[1,*] AND ELENA SEMENETS[2]

[1]School of Earth and Ocean Sciences, University of Victoria, Victoria, B.C., V8W 3P6, Canada
[2]Gemological Research Inc., Vancouver, B.C., Canada

ABSTRACT

Diamond oxidation experiments were undertaken in a piston-cylinder apparatus at 1150 to 1500 °C and 1 GPa to understand the mechanism of diamond oxidation in kimberlite melts and to determine the main rate-controlling parameters for this process. Only surface graphitization, and no diamond resorption, occurs in melts that are fluid undersaturated (synthetic kimberlite, carbonate melt, alkaline basalt, CaO-MgO-SiO_2-H_2O-CO_2 melts). In contrast, fluid oversaturated conditions (as evidenced by the presence of bubbles) produce resorption features commonly seen in natural diamonds recovered from kimberlites. The diamond oxidation rate is the same in the melts with a free fluid phase, in a pure H_2O or CO_2 fluid, suggesting that the process of diamond oxidation is its reaction with the fluid and not with the melt. Both CO_2 and H_2O oxidize diamonds at a similar rate, but produce very different surface features. Therefore, the surface features of natural kimberlite-hosted diamonds may provide information on the relative proportion of H_2O and CO_2 in the kimberlitic fluid. The common diamond morphologies imply significant amount of H_2O. The absence of diamonds with surface graphitization and the abundance of resorbed diamonds in kimberlites suggest the presence of a free fluid phase in kimberlite magmas for hours or days. We found no correlation between the rate and character of diamond oxidation and the physical properties of diamonds (nitrogen content, color).

Keywords: Diamond oxidation, resorption features, experiments, kinetics, fluid phase, kimberlite magmas, nitrogen content

INTRODUCTION

Natural diamonds have ubiquitous resorption features on their surfaces produced by interaction with their host magma during ascent (e.g., Robinson et al. 1989). The resorption results from diamond oxidation into CO_2 (Arima 1998) has a significant impact on the diamond grade and the quality of stones of a kimberlite pipe, and it may bear on their ascent and emplacement history. Many of the resorption features observed in natural diamonds have been produced by experiment (e.g., Chepurov et al. 1985; Kozai and Arima 2005; Sonin et al. 2002), but the mechanism of this process is not completely understood yet. To determine the main rate-controlling factors for diamond oxidation and to be able to predict the degree of diamond preservation in a kimberlite pipe, it is necessary to understand the mechanism of diamond oxidation in kimberlite magmas.

Experimental studies have shown a significant increase in the diamond oxidation rate with temperature (T) and oxidation state (f_{O_2}) (Cull and Meyer 1986; Evans and Phaal 1961; Kozai and Arima 2005; Sonin et al. 2000), which is also borne out in a general way in some natural kimberlites (Fedortchouk et al. 2005). The experiments by Kozai and Arima (2003) quantified the effect of T. A recent experimental study by Kozai and Arima (2005) on diamond dissolution in kimberlite and lamproite melts at 1 GPa shows significant change in the diamond dissolution rate between f_{O_2} fixed by hematite-magnetite (HM) equilibrium and iron-wustite (WI) equilibrium. All the previous experiments on diamond oxidation at controlled f_{O_2} involved etching in gases at 100 kPa, but the results vary significantly among the different studies (Cull and Meyer 1986; Evans and Phaal 1961; Sonin et al. 2000). It is not also known whether diamond oxidation in gases proceeds by the same mechanism as in melts.

Much experimental work has focused on reproducing the many different surface resorption features found on natural diamonds by etching at variable T, pressure (P), and H_2O content (e.g., Chepurov et al. 1985; Zhimulev et al. 2002) and in different melt compositions (Sonin et al. 2002). Nevertheless, the effect of each of those individual variables on the mechanism of diamond dissolution in kimberlite melts, or on the development of various surface etching forms, is not completely understood.

Diamond oxidation produces CO_2 and CO as the final products, and at certain conditions, it is accompanied by surface graphitization of diamonds (Evans and Phaal 1961). Surface graphitization is observed in some diamond dissolution experiments (Chepurov et al. 1985; Sonin et al. 1997) at temperatures much lower than those required for "true" graphitization and is believed to result from oxidation (Davies and Evans 1972; Evans and Phaal 1961). Graphitization is extremely rare on diamonds recovered from kimberlites (Wagner 1914; Tolansky 1968). The diamond oxidation into CO_2 is a commonly accepted process of diamond dissolution (e.g., Arima 1998). Arima (1998) and Kozai and Arima (2005) suggested that kimberlite melt dissolves

* E-mail: dcanil@uvic.ca

0003-004X/07/0007–1200$05.00/DOI: 10.2138/am.2007.2416

diamond in the form of CO_2 and therefore CO_2 solubility in the melt controls the diamond dissolution rate. The CO_2 solubility depends on f_{O_2} and the composition of the melt (Kozai and Arima 2005). Rudenko et al. (1979) argued that the physical dissolution of diamond in the melt is energetically impossible due to the very high energy required to break the three C-C bonds on the surface of the diamond lattice (Rudenko et al. 1979) and contended that only chemical oxidation through the diamond interaction with molecules of volatiles (e.g., CO_2, H_2O, CH_4, CO, etc.) is energetically possible. They therefore suggested that kimberlite melt itself cannot dissolve a diamond, but rather that the reaction with the fluid phase is required for the oxidation to proceed.

In the present study we have explored the effect of fluids on diamond resorption in kimberlite-magma systems (melt and/or fluid). We performed a series of diamond-oxidation experiments in several synthetic compositions with various amounts of H_2O and CO_2 and the conditions close to the experiments of Kozai and Arima (2005). We demonstrate that oxidation in volatile-undersaturated melts results in surface graphitization of diamonds, not their resorption. The presence of a free fluid phase is required to produce the resorption features observed on natural diamonds. We further investigate the kinetics of diamond oxidation, the changes in diamond morphology, and the character of etch-surface features produced by oxidation of diamond in H_2O and CO_2 fluids.

Our results allow us to discuss the mechanism of diamond oxidation in kimberlites and to propose what determines the crystal morphology of a resorbed diamond, orientation and shape of etch pits and resorption forms on its surface. We further apply our results to characterize the fluid regime in kimberlite magmas.

Methods

Both cubic plates and octahedral diamonds were used in the experiments. The plates (edges vary between 0.5–1.3 mm, ~1 mg) were cut from natural inclusion-free diamonds predominantly of IIa type (nitrogen-free). The octahedrons were selected from the <1 mm population from three Lac de Gras kimberlites, and are flat-faced crystals (1–2 mg) with no to little resorption, inclusions or cracks visible in an optical microscope. The octahedra are IaAB and IaB type and with variable color (Table 1). The diamonds were washed ultrasonically for 5 minutes in alcohol before and after each experiment.

The diamond-oxidation experiments were conducted using synthetic compositions of natural aphanitic Jericho kimberlite (JD-82 from Price et al. 2000), natural Kettle River alkali basalt (Brearley and Scarfe 1986), and a simple system CaO-MgO-SiO_2 kimberlite (volatile-free and with H_2O added) (Table 2). To do the experiments above the liquidus, we subtracted 10 wt% of forsterite from JD-82 kimberlite composition. Platinum capsules were used to contain volatiles. For this reason, FeO was replaced by CoO in both the kimberlite and alkaline basalt compositions to avoid Fe loss. The amounts of volatiles were modified to have them completely dissolved in the kimberlite (JK-4) and alkali-basalt (KR13-3) melts during the experiments. A second alkali basalt composition (KR13-1) was prepared without volatiles. To prepare all synthetic compositions, reagent grade SiO_2, TiO_2, Al_2O_3, MgO, CoO, MnO, $CaCO_3$, K_2CO_3, and Na_2CO_3 were ground under alcohol, decarbonated at 850 °C, and fused to a glass at 1500 °C. The glass was then crushed and ground in a mortar, and H_2O and CO_2 were added as brucite and $CaCO_3$. The glasses were analyzed by electron microprobe (EMP) and the amount of volatiles in the final mixture was tested by loss on ignition at 900 °C overnight. The oxidation experiments in pure H_2O fluid were loaded with brucite and run at temperatures above the reaction $Mg(OH)_2 = MgO + H_2O$. For the experiments in CO_2 fluid, a mixture of $CaCO_3$ and SiO_2 was run at temperatures above the reaction $CaCO_3 + SiO_2 = CaSiO_3 + CO_2$. At the run conditions, the kimberlite (JK-4) and alkaline-basalt (KR13-1, KR13-3) compositions were above the liquidus. The compositions in the CMS system at 1400 °C consisted of glass with a few olivine grains at the bottom and, at 1350 °C, glass with olivine crystals making up about one-third of the charge. In this latter composition, the f_{O_2} during experiments was estimated by adding ~2 wt% of V_2O_5 to the mixture (composition CMSV-12/10 in Table 2). The f_{O_2} sensitive partition of V between the co-existing olivine and glass was measured by EMP, and f_{O_2} values near the nickel–nickel oxide (NNO) buffer were then calculated from Canil and Fedortchouk (2001) (Table 3).

For each experiment, about a third amount of the starting mixture was packed at the bottom of a 3 mm diameter Pt capsule. The starting diamonds were photographed under an optical microscope from all sides and then weighed on a microbalance. One or two diamonds were then loaded and the remaining mixture was packed around the crystals. The amount of starting mixture in each run (0.03–0.06 g) was enough to produce oxygen for a complete oxidation of the whole diamond (0.001–0.002 g each). The capsule was sealed by arc welding and loaded in the pressure assembly. The capsule was weighed before and after the welding to ensure that no volatiles were lost.

The diamond oxidation experiments were conducted at 1150–1500 °C and 1 GPa in a piston-cylinder apparatus with 12.5 mm NaCl/pyrex assemblies. For pressure calibration, we used the transition of Ca-Tschermak pyroxene to anorthite-gehlenite-corundum assemblage at 1300 °C and 1.3 GPa and 1400 °C and 1.4 GPa (Hays 1966a). The Ca-Tschermak pyroxene was prepared after Hays (1966b). The calibration showed less than 5% friction correction required for this assemblage, similar to the 3% suggested by McDade et al. (2002). Therefore, we did not apply any friction correction to any experiments and the real pressure was slightly below 1 GPa. Temperature was measured with a $W_{95}Re_5$-$W_{74}Re_{26}$ thermocouple, the accuracy of which was confirmed by the method of Watson et al. (2002). For each experiment, the sample was brought to the final run pressure at 300 °C, heated to 600 °C, and held for 6 min, and then brought to the final run temperature. The pressure was adjusted during the heating, and after the run temperature was reached, no more adjustments of the pressure were made. Quenching was achieved by terminating the power to the graphite furnace. The capsule and the matrix were closely studied after each run. An expanded capsule, release of traces of water during opening the capsule, wet MgO powder, or an abundance of large bubbles in the glass for CMS compositions were used as criteria for the presence of fluid in the experiments.

Each diamond was used in three to five subsequent experiments. In a few failed runs, the fluid was lost and the diamond developed surface graphitization. The graphite was then removed in a short (20 or 30 min) run and the diamond was then used in the following experiments. After each run, the weight loss of the diamond was measured on a microbalance (±0.02 mg). To avoid the effect of the variation in the starting weight of different diamonds on their oxidation rate, we calculated the oxidation rate as mg/mm^2·min, since the use of mg/min and mm/min overestimate oxidation rate for larger stones, and wt%/min for smaller stones. For diamond plates, the change in the surface area was obtained by measuring their three dimensions under an optical microscope. For the octahedral crystals, the surface area was calculated from their weight, density (3.52 mg/mm^3) and the shape. The shape was assumed to be a perfect octahedron for unresorbed stones and a perfect sphere after 40% of the initial weight was lost. The surface area then was calculated proportionally to the weight loss. After some experiments, octahedral diamonds were photographed under the optical microscope and the decrease of the surface area of the octahedral {111} face was calculated using ImageJ software. The diamond surfaces were studied under an optical microscope and scanning electron microscope.

EMP analyses of starting compositions and olivines and glasses in V-doped experiments were done with a CAMECA SX50 electron microprobe at the University of British Columbia with 15.04 kV accelerating voltage, 20.1 nA beam

Table 1. Properties of natural octahedron diamonds used in the oxidation experiments

Diamond	IaA NA (2 atoms) ppm	IaB NB (4 atoms) ppm	N total, ppm	Color/ Intensity
M31	nd	nd	nd	colorless
M83	nd	nd	nd	colorless
M17	nd	nd	nd	colorless
M45	4.10	30.77	34.87	dark brown
M41	0.74	34.28	35.01	yellowish-green
M39	1.26	34.46	35.72	light yellowish-green
M34	3.67	36.78	40.45	colorless
M32	5.04	39.21	44.25	colorless
M63	0.54	47.64	48.17	colorless
F4	263.01	276.91	539.92	colorless
P2	192.00	420.00	612.00	colorless
M57	167.18	891.75	1058.93	colorless
M4	32.70	1165.79	1198.50	intense yellow
M56	235.37	994.46	1229.83	light brown

Table 2. Starting compositions

Oxide	JK-4	KR13-1	KR13-3	CMS-1	CMS-12/3	CMS-12/5	CMS-12/10	CMSV-12/10
SiO_2	32.11	45.40	45.27	56.47	44.09	43.60	42.12	40.57
TiO_2	0.97	2.73						
Al_2O_3	2.36	17.63	15.86					
CoO	9.03	13.41	12.19					
MnO	0.17	0.15						
MgO	23.80	7.29	6.71	19.17	28.38	28.41	27.07	27.15
CaO	20.91	10.78	9.82	19.87	17.53	15.99	15.31	15.30
Na_2O	0.30	0.07	2.98					
K_2O	0.85	0.86	1.16					
V_2O_5	0.00							1.80
H_2O	6.51		3.00	4.50	10.00	12.00	15.50	15.18
CO_2	2.99		3.00					
Total	100.00	98.31	100.00	100.00	100.00	100.00	100.00	100.00

Notes: JK-4 = modified Jericho aphanitic kimberlite JD-82 (from Price et al. 2000); KR13-1 and KR13-3 = natural alkali basalt modeled after Brearley and Scarfe 1986; CMS-1, CMS-12/3, 5, 10, and CMSV-12/10 = a simple system CaO-MgO-SiO_2-H_2O kimberlite.

current, and 1 μm beam size. The counting time on peaks was 20 s for major elements and 100 s for V in olivines. Data reduction was done with the "PAP" $\phi(\rho Z)$ method (Pouchou and Pichoir 1985). Natural and synthetic standards were used for calibration.

Diamond properties

The octahedron diamonds were studied for the presence of fluorescence under UV light, color and color intensity, nitrogen content, and aggregation state (Table 1). The nitrogen content and aggregation states were calculated by deconvolution of FTIR absorbance spectra of whole stones. The spectra were collected using an Avatar 360 FTIR spectrometer at European Gemological Laboratories, Vancouver, at a resolution of 4 cm^{-1}. The spectra were deconvoluted using the method described in Hayman et al. (2005).

There are two types of diamonds in our experiments: IaB type with the a low total nitrogen content (NT) and a high proportion of aggregation centers B (nitrogen forms mainly 2 atom clusters), and IaAB that have both types of aggregation centers A and B (nitrogen forms 4 and 2 atom clusters) (Table 1). For the majority of the experiments we used colorless diamonds without fluorescence. One brown stone with a high nitrogen content, one brown stone with a low nitrogen content, two yellow octahedra, and one intensive yellow hexoctahedron were used to compare the character of oxidation of diamonds with different physical properties.

Results

Resorption vs. surface graphitization

The experiments in volatile-undersaturated compositions (i.e., no free fluid) developed surface graphitization on diamonds (Table 4). Graphite was in various forms: a layer covering the entire stone, separate spots with a frosted diamond surface in between, individual graphite crystals on the frosted diamond surface, and pockets with long needle-like crystals of graphite. At 1450 and 1500 °C, the diamond loses weight and is replaced by graphite, whereas at 1350 °C, the diamond gains weight by graphitization, likely due to the rapid migration of C from the graphite heater through the Pt capsule into the sample during the experiment (Watson 1987). After the removal of the graphite layer in a mixture of HNO_3 and H_2SO_4 acids heated at 200 °C, the diamonds show the irregular corrosion structures described in Sonin et al. (1997). An increase in the CO_2 content of KR13-3 basalt (by addition of a $CaCO_3$ layer at the bottom of the capsule) resulted in suppressing the graphitization (Table 4), but experiments in $CaCO_3$ alone produced a thick graphite layer on the diamond.

Table 3. Olivine and glass compositions in experiments in CMSV-12/10 mixture and the f_{O_2} values calculated from $D_V^{ol/gl}$ after (Canil and Fedortchouk 2001)

Sample	MgO	SiO_2	CaO	V_2O_5	Total	$D_V^{ol/gl}$	ΔNNO*	logf_{O_2}†	ΔWM†
P245-gl	30.3	48.9	16.84	2.01	98.1	0.042	–0.2	–5.9	0.8
P245-ol	57.6	42.3	0.33	0.09	100.3				
P246-gl	27.8	49.7	17.60	2.01	97.1	0.056	–0.6	–6.4	0.3
P246-ol	57.0	42.7	0.35	0.11	100.2				
P248-gl	30.1	49.7	17.78	2.01	99.6	0.029	0.5	–5.2	1.5
P248-ol	57.3	42.2	0.34	0.06	99.9				
P256-gl	28.1	47.9	18.75	1.67	96.4	0.043	–0.2	–5.9	0.8
P256-ol	56.4	43.4	0.37	0.07	100.2				
P280-gl	29.9	48.7	18.30	1.68	98.6	0.040	–0.1	–5.8	0.9
P280-ol	56.9	42.8	0.35	0.07	100.1				
Average						0.042	–0.1	–5.8	0.9

* Calculated from logD_V= –0.24ΔNNO –1.41 (Canil and Fedortchouk 2001).
† The equations for NNO and WM buffers are from Frost (1991).

Experiments in volatile-oversaturated compositions produced no graphitization on diamond, but resorption similar to that produced naturally in kimberlites and in other diamond dissolution experiments (Table 4). Cubic diamond plates developed square etch pits on {100} faces and rounding of the corners and edges (Fig. 1d). Octahedra developed trigon etch pits on {111} faces. Rounding of their edges and corners to a change in the morphology from octahedron to hexoctahedron, and development of striation features on the growing hexoctahedra faces (Fig. 2). The final morphology of a diamond that lost more than 40 wt% is a hexoctahedron with striations on all the sides (Fig. 2d), typical of natural diamonds in kimberlites.

The effect of the presence and the amount of a free fluid phase on diamond oxidation is evident in the CMS synthetic kimberlite experiments (Fig. 1). CMS kimberlite is close to the composition of diopside that reaches H_2O-saturation at 10 wt% H_2O in the melt at pressure of 1 GPa (Eggler and Burnham 1984). Therefore, we expect CMS kimberlite with 5 wt% of H_2O to be water-undersaturated and CMS with ≥12 wt% of H_2O to have a free fluid phase present during the runs. This agrees well with the amount and distribution of bubbles in the run products of the experiments in CMS kimberlite (Fig. 1). Minor interstitial glass and significant proportion of olivine crystals make the composition with 5 wt% H_2O very different from those with higher water contents. The similarity of run products formed in the CMS system with 10, 12, and 15 wt% H_2O suggests that at

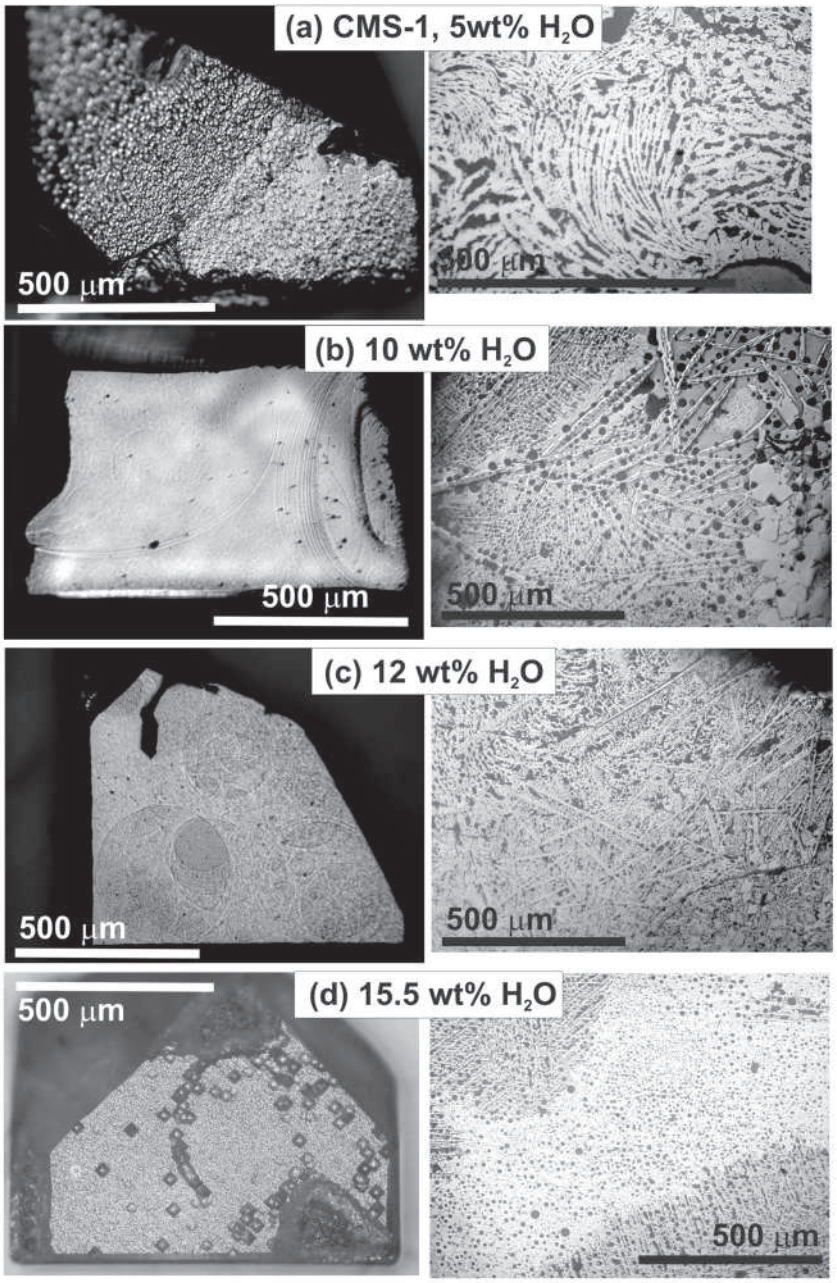

FIGURE 1. Diamond surface after oxidation experiments in melts with variable amounts of fluid. The coexisting matrix around the diamond with the amount and structural position of the bubbles is shown for each experiment. All photographs were taken with an optical microscope. (**a**) H_2O-undersaturated melt (bubbles only form during quench, i.e., along the quench crystals) and diamond develops surface graphitization; (**b**) at the H_2O-saturation limit or slightly above (abundant large bubbles on quench crystals and between the olivine crystals), no etch pits formed, almost no visible resorption, disk forms on diamond surface; (**c**) very small amount of free fluid, produces surface etching, small rare etch pits; (**d**) more fluid (bubbles in the glass), produces widespread development of etch pits.

TABLE 4. Results of diamond oxidation in different compositions

Composition	H_2O (wt%)	CO_2 (wt%)	*T* (°C)	Surface graphitization	Resorption	Bubbles in the matrix
JK-4	6.5	3	1500	layer	weight loss	absent
KR13-1	0	0	1300	minor	no	absent
KR13-3	3	3	1200	spots	no	absent
KR13-3	3	3	1400	thin layer	no	absent
KR13-3 + $CaCO_3$	3	>3	1200	absent	no	bubbles/quench
$CaCO_3$			1450	extensive	undetermined	
$CaCO_3$			1500	extensive, spots	undetermined	
CMS-1	5		1400	layer	undetermined	bubbles/quench
CMS-1 + H_2O	12–13		1400	absent	resorption, pits	bubbles
CMS-12/10	15.5		1400	absent	resorption, pits	bubbles
CMS-12/5	12		1400	absent	minor, small pits	bubbles
CMS-12/3	10		1400	absent	no resorp., disks	bubbles
CMSV-12/10	15.5		1350	absent	resorption, pits	bubbles
Mg(OH)2	100		1150–1350	absent	resorption, pits	
$CaCO_3$ + SiO_2		100	1250–1350	absent	resorption, pits	

10 wt% H_2O, some free fluid was probably present during the run. In CMS kimberlite with 5 wt% H_2O, all fluid is in the melt (i.e., no free fluid phase) resulting in surface graphitization (Fig. 1a). The same composition with 10 wt% of H_2O, just above the fluid-saturation limit, produces no resorption, but large circular features on the diamond surface (Fig. 1b), usually referred to as disks (Afanasiev et al. 2000). A further increase in the H_2O content resulted in square etch pits usually present on the {100} face in natural diamonds (Figs. 1c and 1d). Higher H_2O contents favor larger etch pits (Figs. 2a, 2b, and 3).

Character and rate of diamond oxidation in different media

The effect of fluid composition on diamond oxidation was studied in pure H_2O and CO_2 fluids. Carbon migration into the capsule during the experiments likely produced some C-bearing volatile species in the H_2O runs (Watson 1987). Although a Pyrex sleeve in our pressure assembly significantly decreases H_2 migration through the walls of the Pt capsule into the sample, some H_2O in the runs with CO_2 fluid is still possible. When normalized to the surface area of the diamond, there is a similar rate of weight loss (within the uncertainties) for several diamonds oxidized in H_2O, CO_2, and CMSV-12/10 melt at the same conditions (Fig. 4a). The composition of the fluid (H_2O or CO_2) does not effect the rate of diamond oxidation at different T (1250, 1350 °C) (Table 5).

Diamond resorption can also be expressed as a decrease of the area of primary octahedron faces {111} during transformation into the secondary hexoctahedron. For the same amount of weight loss, diamonds etched in H_2O develop more profound resorption of the octahedron form than those etched in CO_2 (Figs. 2b, 2c, 2e, and 2f). Numerically, this difference is shown as a relationship between the preservation of the initial area of all octahedron faces or their remnants, and the preservation of the

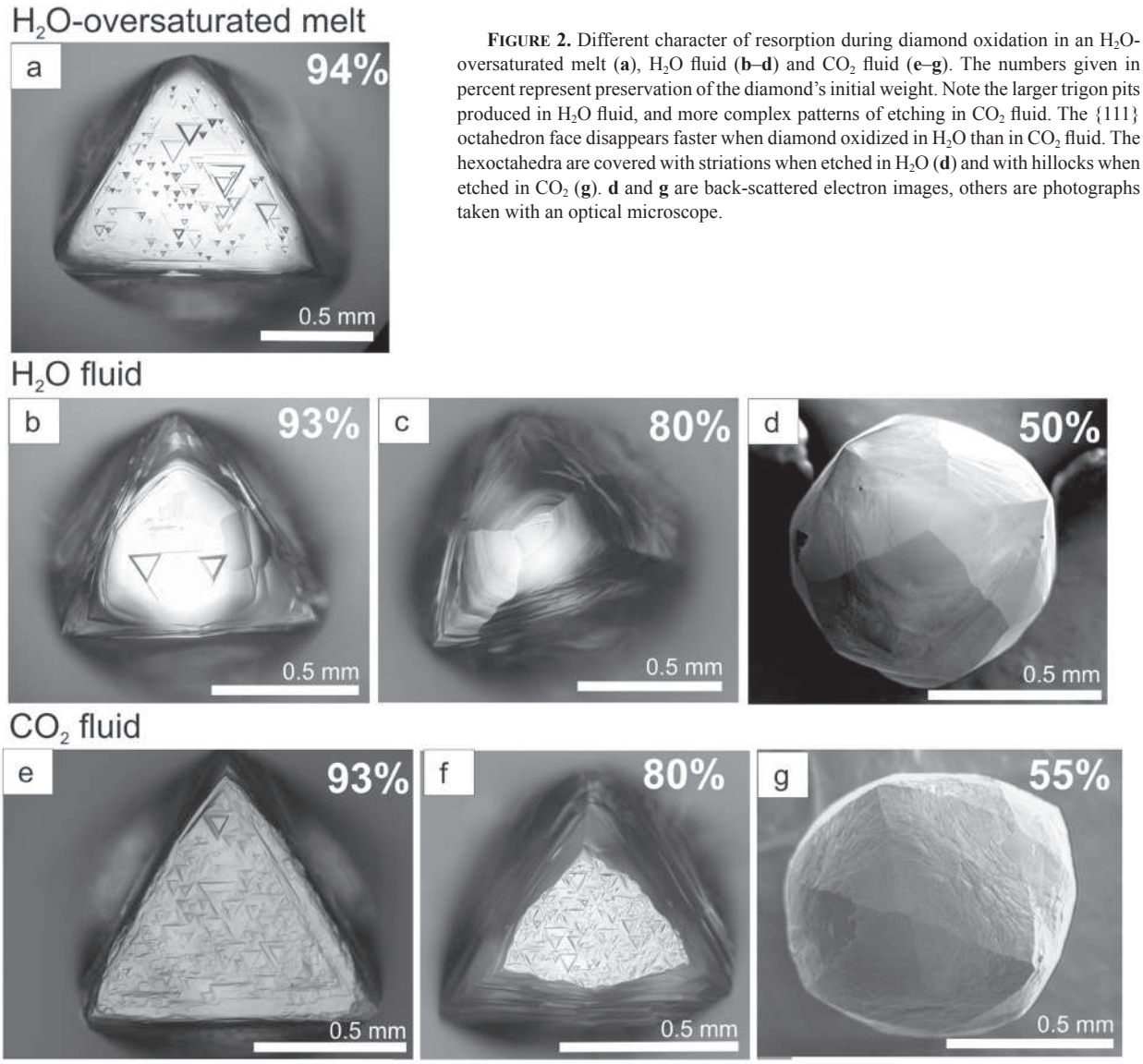

Figure 2. Different character of resorption during diamond oxidation in an H_2O-oversaturated melt (**a**), H_2O fluid (**b**–**d**) and CO_2 fluid (**e**–**g**). The numbers given in percent represent preservation of the diamond's initial weight. Note the larger trigon pits produced in H_2O fluid, and more complex patterns of etching in CO_2 fluid. The {111} octahedron face disappears faster when diamond oxidized in H_2O than in CO_2 fluid. The hexoctahedra are covered with striations when etched in H_2O (**d**) and with hillocks when etched in CO_2 (**g**). **d** and **g** are back-scattered electron images, others are photographs taken with an optical microscope.

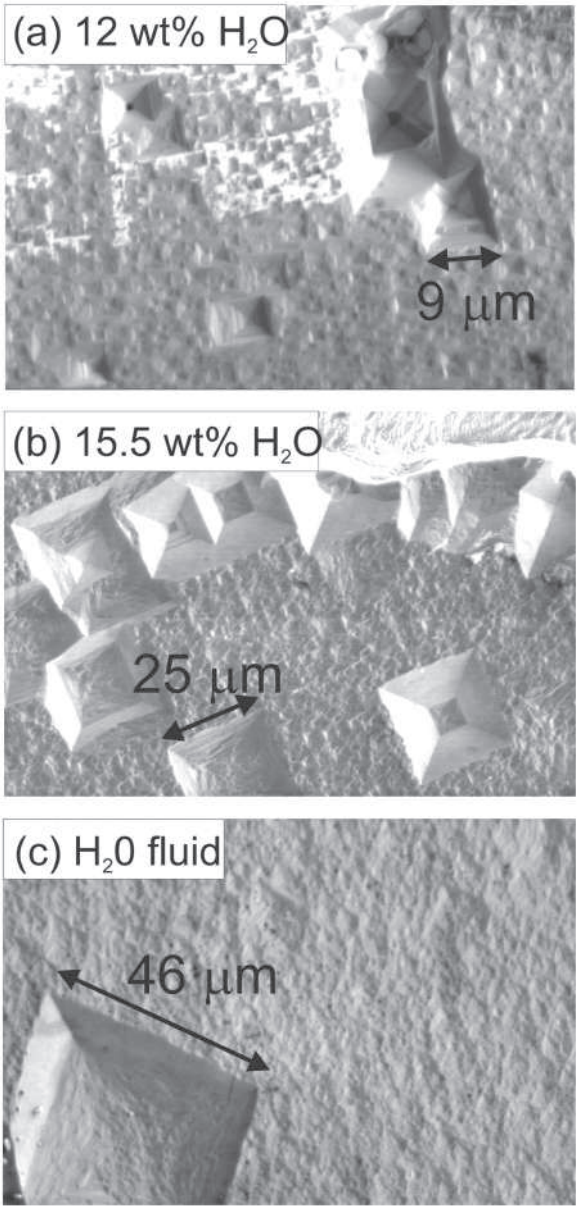

FIGURE 3. Enlargement of the etch pits with an increase of H_2O content of the melt (back-scatter electron images).

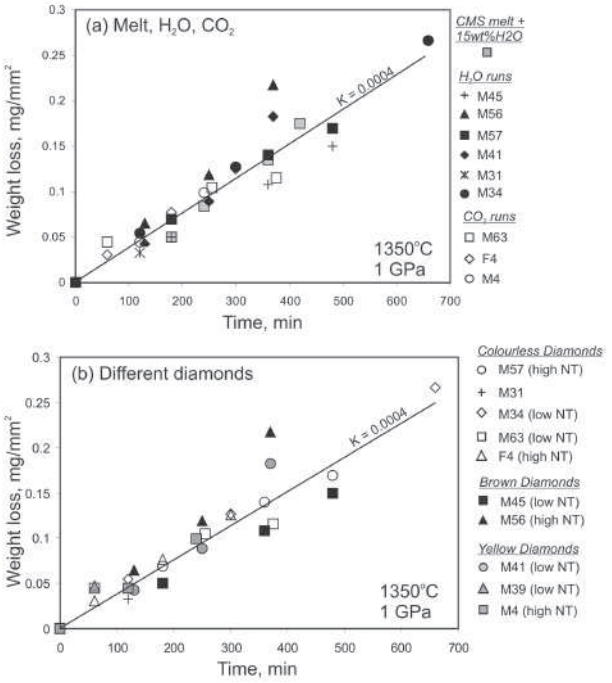

FIGURE 4. Oxidation rate of natural octahedron diamonds in the experimental runs at 1350 °C and 1 GPa in piston-cylinder apparatus. The plot shows no differences in the kinetics of diamond oxidation in different reagents (**a**) and for diamond with various properties (**b**). The two points with the higher oxidation rate on both plots are from the same experimental run, which might have slightly different conditions. Low and high nitrogen content of the diamonds indicated as NT (total nitrogen). All error bars are smaller than the size of the symbols.

diamond's initial weight for several experimental runs (Fig. 5). The areas were measured on enlarged photographs of individual faces under an optical microscope before and after experiments, calculated by ImageJ software, and averaged for each stone. For diamonds with only a few faces photographed, only the faces where photographs were obtained for each run were used. We considered the octahedron face disappeared completely when no remnant of this face was observed under the microscope. There is much faster disappearance of octahedron faces in H_2O than in CO_2 (Fig. 5). The change in the rate of loss for the M32 and M56 diamonds was due to the fluid loss in the second run and development of surface graphitization that decreased the weight without changing the morphology of the diamond. After the removal of the graphite layer in the subsequent run, the rate of {111} face

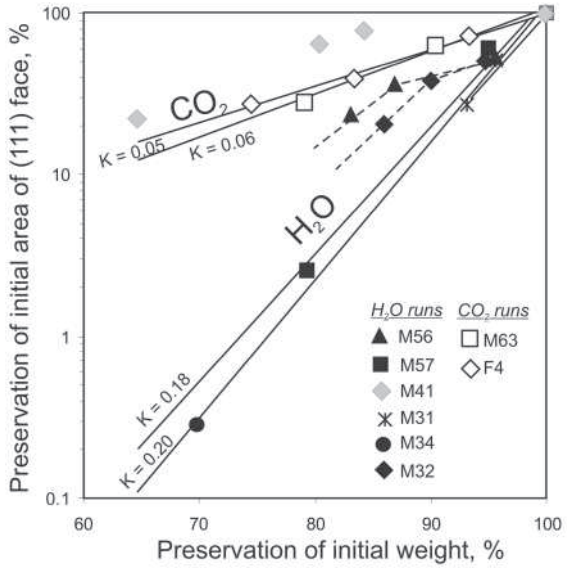

FIGURE 5. Decrease in the area of {111} octahedron face of the initial diamond vs. the initial weight loss during oxidation in H_2O and in CO_2 fluids showing longer preservation of the diamond's primary morphology in CO_2 fluid. Change in slope in M32 and M56 lines is due to surface graphitization between the second and following runs.

TABLE 5. Experimental conditions and results of diamond oxidation experiments at 1 GPa

Run no.	Diamond	Composition	*T* (°C)	Duration (min)	Initial weight (mg)	Weight loss (mg)*	Total preservation (wt%)†	Area (mm^2)‡	Area weight loss (mg/mm^2)	Preserved {111} face (%)§
					Runs in fluid undersaturated melts					
P-220	plate	KR13-1	1300	30	1.4					
P-221	plate	JK-4	1500	30	0.8					
P-222	plate	JK-4	1500	90						
P-226	plate 25	KR13-3	1200	60	1.1					
P-228	plate 32	KR13-3	1400	64	0.8					
P-227	plate 31	KR13-3 + Cc	1200	60	0.7					
P-229	plate 35	$CaCO_3$	1450	30	0.53					
P-230	plate 38	$CaCO_3$	1500	30	0.6					
P232	plate	CMS-1	1400	30						
					Runs in melt with free fluid phase					
P235	plate	CMS-1 + H_2O	1400	30						
P238	plate	CMS-12/10	1400	30						
P239	plate	CMS-12/5	1400	30						
P240	plate	CMS-12/3	1400	30						
P241	plate	CMS-12/10	1350	60						
P244	plate	CMSV-12/10	1350	60						
P245	M32	CMSV-12/10	1350	60	1.98	0.11	94	3.90	0.028	48.9
P246	M57	CMSV-12/10	1350	60	2.02	0.1	95	3.95	0.025	60.4
P247	M45	CMSV-12/10	1350	60	1.04	–0.06	106	2.54	–0.024	
P248	M56	CMSV-12/10	1350	60	1.59	0.07	96	3.37	0.021	52.4
P252	M45	CMSV-12/10	1350	120	1.1	0.09	97	2.54	0.035	
P254	M41	CMSV-12/10	1350	60	1.33	0.21	84	2.99	0.070	77.6
P256	M34	CMSV-12/10	1350	120	2.15	0.11	95	4.12	0.027	49.5
P-280	M32	CMSV-12/10	1350	120	1.78	0.08	86	3.49	0.023	20.4
					Runs in H_2O fluid					
P249	plate	$Mg(OH)_2$	1350	60	1.11	0.37	67	nd	nd	
P250	M31	$Mg(OH)_2$	1350	120	1.61	0.11	93	3.40	0.032	28.1
P258	M34	$Mg(OH)_2$	1350	20	2.04	0.08	91	4.04	0.020	
P259	M34	$Mg(OH)_2$	1350	120	1.96	0.21	81	3.87	0.054	
P260	M34	$Mg(OH)_2$	1350	180	1.75	0.25	70	3.44	0.073	0.3
P-263	M34	$Mg(OH)_2$	1350	360	1.5	0.41	51	2.94	0.139	
P-264	M45	$Mg(OH)_2$	1350	180	0.91	0.11	77	2.19	0.050	
P-266	M45	$Mg(OH)_2$	1350	180	0.8	0.11	66	1.92	0.057	
P-275	M45	$Mg(OH)_2$	1350	120	0.69	0.07	60	1.67	0.042	
P-264	M57	$Mg(OH)_2$	1350	180	1.85	0.25	79	3.61	0.069	2.6
P-266	M57	$Mg(OH)_2$	1350	180	1.6	0.22	68	3.11	0.071	
P-275	M57	$Mg(OH)_2$	1350	120	1.38	0.08	64	2.69	0.030	
P-273	M41	$Mg(OH)_2$	1350	130	1.07	0.11	72	2.37	0.046	
P-274#	M41	$Mg(OH)_2$	1350	120	0.96	0.1	65	2.15	0.047	22.0
P-276	M41	$Mg(OH)_2$	1350	120	0.86	0.18	51	1.93	0.093	
P-273	M56	$Mg(OH)_2$	1350	130	1.32	0.18	72	2.78	0.065	
P-274	M56	$Mg(OH)_2$	1350	120	1.14	0.13	64	2.40	0.054	
P-276	M56	$Mg(OH)_2$	1350	120	1.01	0.21	50	2.14	0.098	
P-292	P2	$Mg(OH)_2$	1250	330	1.88	0.09	95	3.76	0.024	
P-294	P2	$Mg(OH)_2$	1250	360	1.79	0.08	91	3.58	0.022	
P-296	P2	$Mg(OH)_2$	1250	360	1.71	0.1	86	3.41	0.029	
P-298	M83	$Mg(OH)_2$	1150	2700	1.19	0.04	97	2.68	0.015	
					Runs in CO_2 fluid					
P-285	plate 42,46	$CaCO_3 + SiO_2$	1350	60	1.45	0.41	72	nd	nd	
P255	plate 43	$CaCO_3 + SiO_2$	1350	60	0.6	0.17	72	2.012	0.084	
P255	M63	$CaCO_3 + SiO_2$	1350	60	1.58	0.15	91	3.35	0.045	64.9
P-269	M63	$CaCO_3 + SiO_2$	1350	195	1.43	0.18	79	3.02	0.060	28.3
P-277	M57	$CaCO_3 + SiO_2$	1350	120	1.3	0.18	55	2.54	0.071	
P-278#	M39	$CaCO_3 + SiO_2$	1350	60	2.09	0.19	91	4.04	0.047	
P-278	F4	$CaCO_3 + SiO_2$	1350	60	1.33	0.09	93	2.99	0.030	71.9
P-279	F4	$CaCO_3 + SiO_2$	1350	120	1.24	0.13	83	2.78	0.047	40.0
P-282	F4	$CaCO_3 + SiO_2$	1350	120	1.11	0.12	74	2.48	0.048	27.2
P-279	M4	$CaCO_3 + SiO_2$	1350	120	2.09	0.16	92	3.57	0.045	
P-282	M4	$CaCO_3 + SiO_2$	1350	120	1.93	0.18	84	3.30	0.054	
P-297	M17	$CaCO_3 + SiO_2$	1250	360	2.12	0.08	96	4.08	0.020	

* For graphitized diamonds weight loss is often negative due to gaining graphite.
† Preservation is shown as a per cent from the original octahedron form.
‡ Area is calculated from weight, density and and shape (100% preserved = octahedron, 60% preserved = sphere).
§ Octa face preservation calculated by change in the area of (111) faces.
# The runs when a yellow diamond lost its color.

loss for both diamonds became parallel to the other H_2O-etched stones. The strange behavior of the yellow M41 diamond might be explained by a complex initial surface of this stone covered with many growth and resorption features.

H_2O and CO_2 fluids produce contrasting etch characteristics on diamonds. On the octahedron {111} face (Fig. 2b), H_2O fluid produces a few individual, large flat-bottomed trigons, whereas CO_2 covers the face with numerous smaller point-bottom trigons and few hexagons (Fig. 2e). The increase in the number of hexagons with a decrease in temperature agrees with the observation by Yamaoka et al. (1980). Etching of the cubic face {100} of diamond plates in H_2O and CO_2-rich fluids also creates distinc-

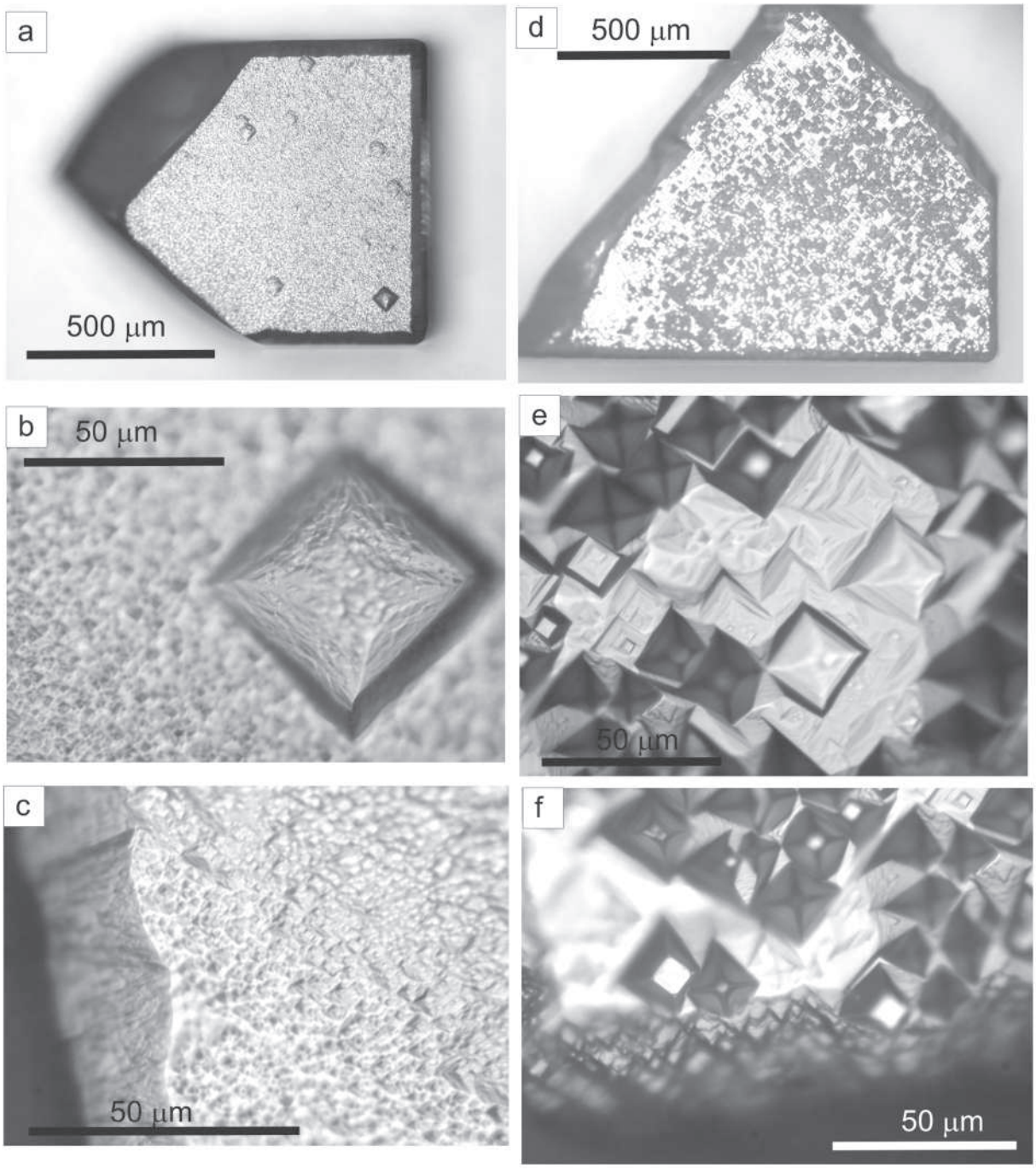

FIGURE 6. Different character of etching of {100} face of a cubic diamond plate in H_2O (run P-249) and CO_2 (run P-285) fluids. Oxidation in H_2O produces few large square pits on intensively etched diamond surface (**a**–**c**), whereas oxidation in CO_2 produces many smaller square pits with more regular shape and pointed-bottom (**d**–**f**). Surface etch features on the diamond edge, {110} direction, also differ between the two fluids (**c**, **f**).

tively different features (Fig. 6). On the hexoctahedra faces, H_2O produces striations along the former octahedron edges, and CO_2 covers the whole surface with slightly elongated drop-shaped irregularities called hillocks (Figs. 2d and 2g). Other features observed only in runs with H_2O fluid are shown in Figures 7a, 7c, 7g, and 7h and those observed only in runs with CO_2 fluid on Figures 7b, 7d, 7e, and 7f. The fluid composition during the most recent etching event dictates the final morphology and overprints the previous features produced in a different fluid. For example, diamond M57 was oxidized in H_2O during five runs, but the final run in CO_2 fluid (P-277 Table 5, 2 hours) resulted in the typical "CO_2 etch surface" (Fig. 2g).

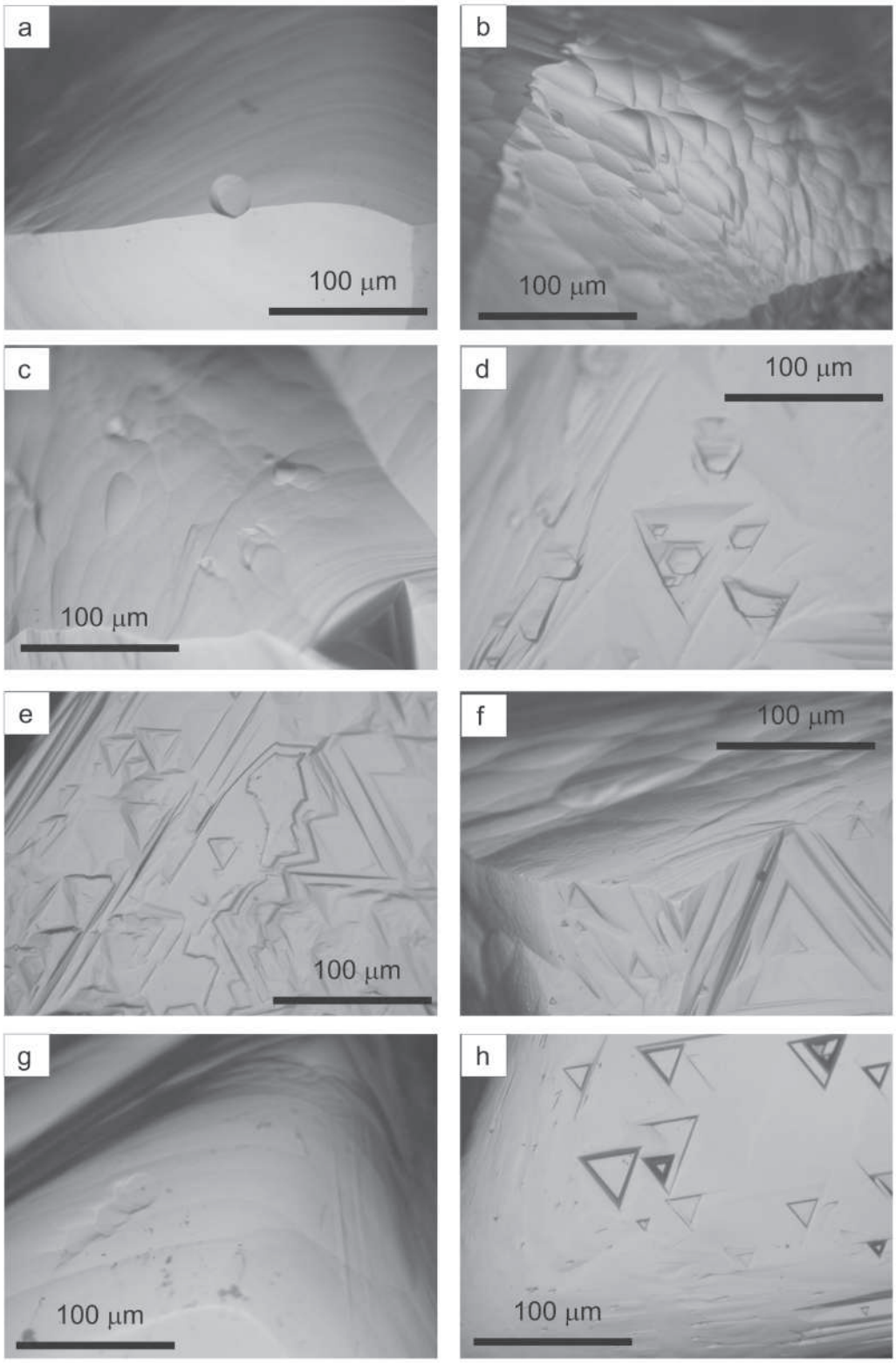

FIGURE 7. Photographs taken with an optical microscope of etch features produced on octahedra after oxidation in H_2O and CO_2 fluids. The most common features produced only in H_2O fluid: (**a**) striation and round cavities on hexoctahedra faces, (**c**) individual round pyramid-shape hillocks, (**h**) small pointed holes, (**g**) deformation lamellae. In CO_2 fluid, the main features are (**b**) drop-shape hillocks completely covering the surface of hexoctahedrons, (**d**) hexagons, (**e**) etch pits of irregular shape, (**f**) rough surfaces.

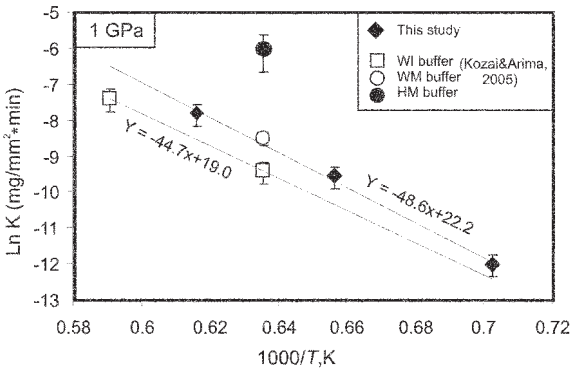

FIGURE 8. Temperature dependence of diamond oxidation rates in H_2O-fluid (this study) and in natural Wesselton kimberlite (Kozai and Arima 2005) at various values of f_{O_2}. Note the good agreement between the two studies both in the slopes [relative to the iron–wüstite (IW) oxygen buffer, Kozai and Arima, 2005, and wüstite–magnetite (WM) buffer, this study] and in diamond oxidation rates at f_{O_2} near the WM buffer. The oxidation rates from Kozai and Arima (2005) were normalized to the surface area of each diamond. The error bars are one standard deviation.

Oxidation of different diamonds

The oxidation rates are similar for all the diamonds and do not vary with color (colorless, light brown, dark brown, light yellow, dark yellow) or nitrogen content (from 35 to 1200 ppm) (Fig. 4b). Two yellow octahedra (M41 and M39) lost their yellow color after one or two runs. The two possible reasons are: (1) color loss at our experimental conditions; and (2) only the outer layer of these stones had a yellow color and it was removed thus making the diamond colorless. The latter explanation is confirmed in two test runs with a diamond having a strong yellow color, hexoctahedra morphology, and a broken side (M4; Table 1) to ensure that the internal part of the diamond is exposed and has the same color as the outer layer. This stone gave the same oxidation rate as the others and no loss or lightening of the color. Surface etch features produced on different stones are similar at the conditions of our experiments.

DISCUSSION

Mechanism of diamond oxidation in kimberlite melt

The results of our experiments suggest that the presence of a free fluid phase is required to produce the resorption features observed in natural diamonds (i.e., the change of the primary octahedron diamond into hexoctahedron and development of etch trigons). Any oxidation reaction by diamond interaction with a volatile species dissolved in a melt or the melt components results in surface graphitization. At the volatile-saturation limit of the melt, we observed no surface graphitization, no changes in diamond morphology, but development of large disk sculptures, similar to those occasionally encountered in natural kimberlitic diamonds (Afanasiev et al. 2000). Thus, the oxidation in the melt just above its volatile-saturation limit causes resorption, but the kinetics of the process at this point is very slow. At conditions in which the melt is sufficiently fluid oversaturated, the resorption proceeds. The character and kinetics of the resorption is the same in volatile-saturated melt as in a pure fluid, but the size of etch pits and their number may vary.

The diamond oxidation rate in our experiments obtained at 1150, 1250, and 1350 °C, 1 GPa and f_{O_2} slightly above WM buffer compares well with the rate recorded by Kozai and Arima (2005) for diamond oxidation in Wesselton aphanitic kimberlite (Fig. 8) oversaturated in volatiles (indications of fluid presence during the runs are described in Kozai and Arima 2005). This consistency between two different studies supports our observation that oxidation in a pure fluid is the same as in the melt-fluid (i.e., magma) systems and represents the process of diamond oxidation in the natural kimberlite magmas.

Since the fluid phase, and not the kimberlite melt, oxidizes diamond, only the conditions of this fluid determine the kinetics of resorption. Kozai and Arima (2005) argued that CO_2 solubility in the melt determines the oxidation rate, because they observed that addition of 30 and 50 wt% $CaMg(CO_3)_2$ to the Wesselton aphanitic kimberlite suppressed the oxidation, and experiments in the pure $CaMg(CO_3)_2$ produced surface graphitization. We suggest an alternative explanation for their observation. Addition of dolomite greatly increases water solubility in the melt (Keppler 2003) and consequently could greatly decrease the amount of fluid in the system to the saturation limit, decreasing the diamond oxidation rate as observed by Kozai and Arima (2005). The surface graphitization produced in dolomite agrees with our data and is caused by the absence of a free (H_2O or CO_2) fluid phase. Kozai and Arima (2005) obtained much slower diamond oxidation in lamproite than in kimberlite. Their lamproite composition had significantly less volatiles than the kimberlite, especially CO_2, which has a lower saturation limit. As a result, this lamproite might not have had enough fluid to fully support the oxidation.

The H_2O–CO_2 fluid system of kimberlite melts (Mitchell 1986) has the following volatile species: H_2O, H_2, CH_4, CO, CO_2 (Holloway and Blank 1994). The mole fraction and the activity of these species in the oxidation reaction with the diamond surface would depend primarily on T and f_{O_2}. It is possible that the components of the melt react with the products of diamond oxidation in the fluid phase (CO_2, H_2) and affect the amount of reagents and products in the diamond oxidation reaction. In this case, the melt composition could affect the oxidation rate, but if this process operates, it probably has a very minor effect. The results of the present study suggest that as long as a melt is fluid-saturated, the T, P, and f_{O_2} of the system will determine the kinetics of diamond oxidation.

Diamond resorption and the development of surface graphitization are the two competitive processes of diamond oxidation. The activation energies for surface graphitization of the {111} and {110} diamond faces are 1059 ± 75 and 728 ± 50 kJ/mol, respectively (Davies and Evans 1972), corresponding to the energy required to break three or two C-C bonds of the diamond lattice (the energy of one bond is 347 kJ/mol, from Rudenko et al. 1979). The activation energy of diamond oxidation by resorption is ~346–427 kJ/mol (Cull and Meyer 1986; Arima and Kozai 2006; and the slope in Fig. 8) and corresponds to the breakage of one C-C bond. Rudenko et al. (1979) argued that the most energetically favorable process of diamond oxidation is the attachment of volatile molecules (H_2O, CO_2, CH_4, etc) to the open carbon bonds on the diamond surface. The reaction of

TABLE 6. Diamond morphology and surface features produced in H_2O and CO_2 fluids at 1350 °C and 1GPa and relative oxidation rate in the different directions of diamond lattice

Resorption features	H_2O fluid		CO_2 fluid	
	surface features	relative oxidation rate	surface features	relative oxidation rate
preservation of primary octahedron shape	fast rounding of crystal	{100}, {110} faster	longer preservation of sharp edges and {111} surfaces	{111} faster
orientation of etch pits	negative	{110} < {100}	mainly negative with some positive features	{110} ≤ {100}
size/shape of etch pits	large, flat-bottom trigons	{111} slow	small, pointed-bottom trigons	{111} fast
density of etching	few trigons on unresorbed {111} face	{111} slow	numerous trigons cover the whole {111} face	{111} fast
features on THH faces	striation		drop-like hillocks	

the components of these molecules with the surrounding C atoms breaks the remaining C-C bonds one by one, to form new C-OH, C-O, C-H… etc. bonds, whose energy of formation is higher than the energy required to break a single C-C bond. These various C-O-H-OH compounds then break down into CO and CO_2, the final products of diamond oxidation. With this process, the C atom detaches from the diamond lattice by breaking only one C-C bond, in agreement with the measured activation energy. Thus, diamond oxidation by H_2O-CO_2 fluid is the fastest process and it produces diamond resorption, whereas in the absence of the fluid, the less energetically favorable oxidation accompanied by surface graphitization proceeds.

What determines the morphology of resorbed diamonds?

At the conditions of our experiments we found no effect of the fluid composition on the kinetics of diamond oxidation, but a great influence on the surface forms and morphology produced by the resorption. In nature, diamond resorption in kimberlite melts produces various surface forms. The most common are negative trigon and square etch pits (with vertices of the pit pointed in a direction opposite to the vertices of the diamond face), the shape, orientation, and number of which greatly vary in natural diamonds. The less-common resorption features are hexagons, disks, cavities, and positive trigons (the pit sides are parallel to the edges of the diamond face). Variation in the degree of volume resorption and surface etching can produce resorbed diamonds with clear untouched remnants of octahedron faces, or well-preserved octahedra completely covered with etch pits. Striations and hillocks are two of the most common etch features on hexoctahedra and show a great variation in shape even within one diamond population (Fedortchouk et al. 2005). The morphological changes in diamonds during resorption affect the yield during diamond cutting, and therefore, the quality of a stone. It is important, therefore, to constrain what determines the final morphology of a resorbed diamond.

Several previous experimental studies found that different solvents and the variation in the H_2O content of melts produce different surface etch features on diamonds (Chepurov et al. 1985; Pal'yanov et al. 1995; Sonin et al. 2002). Yamaoka et al. (1980) studied the influence of T and f_{O_2} on the orientation of trigon etch pits, where negative trigons required lower f_{O_2} and higher T. They suggested that the relative oxidation rates in the {100} and {110} directions determined the pit orientation, whereas at high f_{O_2} and low T, the oxygen forms C-O-C bridges in the {100} direction and stabilizes the oxidation (Yamaoka et al. 1980, and references therein).

The diamond morphologies produced by resorption in H_2O and CO_2 fluids in our experiments differ significantly and are summarized in Table 6. They agree well with Kozai and Arima (2005) and represent the end-members of the surface resorption features produced by diamond oxidation in kimberlite with 6.2 wt% H_2O and 4.8 wt% CO_2 (Figs. 1b, 1d, and 1f in Kozai and Arima 2005). This example shows that the development of the surface resorption features is predictable from the fluid composition, at least for the H_2O-CO_2 system.

Following Yamaoka et al. (1980, and references therein), we explain the diversity of the surface features in our experiments by the differences in the relative oxidation rates in the three main directions of the diamond lattice: {111}, {110}, {100} (Table 6). The cause of the variation in the oxidation rates may be hidden in the differences in the diamond lattice in these three directions. The position and distance between the open bonds in the diamond lattice is different along the {111}, {110}, and {100} directions. Different volatile molecules in an H_2O-CO_2 fluid also vary in size and configuration, and therefore, would probably prefer attachment on certain directions of the diamond lattice. The activity of different volatile species in the fluid would affect the relative oxidation rates in the different directions and, as a result, the diamond morphology. More experimental studies are needed to define the relationship between the activity of volatile species and the relative oxidation rates in the different directions of the diamond structure. Our preliminary experiments show that an increase in the CO_2 content of fluids results in higher oxidation rates in the {111} direction.

Influence of diamond properties on their oxidation

In the Lac de Gras kimberlite pipes, brown diamond populations commonly have a much higher degree of resorption, whereas diamonds from kimberlites with mainly colorless stones are less resorbed (Gurney et al. 2004; Fedortchouk et al. 2005). This may have resulted from a very different history of the diamond populations, or simply from faster resorption of brown diamonds. Mendelssohn and Milledge (1995) suggested that the variation in the amount of defects in the diamond structure such as nitrogen impurities and plastic deformation (the common explanation for the brown color of diamonds), may affect diamond oxidation rates. We tested the effect of diamond properties on their oxidation rate and resultant surface resorption features by putting two different diamonds in the same experimental run, and by repeating runs at the same conditions with different diamonds.

Similar oxidation rates and surface resorption features are observed for low-nitrogen, high-nitrogen, colorless, brown, and yellow stones (Tables 1 and 5, Fig. 4b). If the oxidation rate is affected by the physical properties of a diamond, these differences are within the uncertainties of our experimental method,

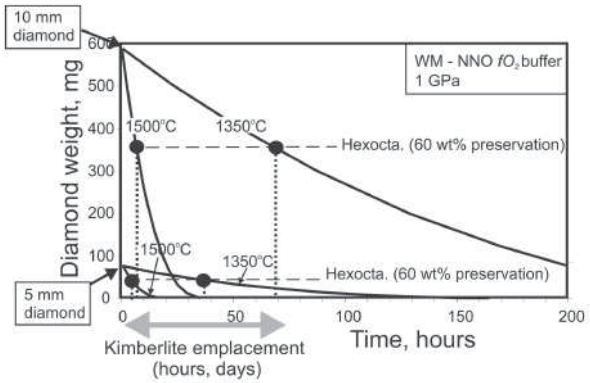

FIGURE 9. Diamond initial weight loss during oxidation at 1350 and 1500 °C, 1 GPa and NNO buffer calculated for an octahedron diamond 10 mm in diameter (dotted lines) and 5 mm diameter (solid lines) by the formula:

$$Weight_{time2}(mg) = Weight_{time1}(mg) - Rate\ (mg/mm^2 \cdot h^{-1}) \times Area_{time1}(mm^2).$$

The oxidation rate at 1350 °C (0.024 mg/mm²·h) is from the present study, at 1500 °C (0.247 mg/mm²·h) is extrapolated from Kozai and Arima (2005) using Arrhenius relationship. The primary octahedron form is completely converted into secondary hexoctahedron after 40% of the initial diamond weight loss and the weight correspondent to the 60% of the initial weight for both diamonds is shown.

and therefore, are very small relative to the effect of T and f_{O_2} on the preservation of diamonds in kimberlites.

Fluid system of the Lac de Gras kimberlites, diamond preservation, and quality

Many lines of petrological evidence indicate a high volatile content for kimberlites. A large amount of carbonates in their groundmass implies a high content of CO_2 in the fluid (e.g., Price et al. 2000). The exact fluid composition of kimberlite melts, however, is not well-constrained due to ambiguity in the primary composition of kimberlites, their protracted emplacement history, the overprint of deuteric alteration, and complex origin of some groundmass carbonates and hydrous minerals. The relationships between diamond morphology and the presence and composition of fluid observed in this study can help us to learn more about the fluid in kimberlite magmas and the proportions of the major volatiles—H_2O and CO_2—during their emplacement.

The presence of hexoctahedra, the secondary diamond morphology produced during resorption, and the absence of diamonds with surface graphitization in the majority of kimberlites requires the presence of a fluid phase during the latest stages of kimberlite emplacement. The only known occurrence of diamonds with surface graphitization is at Premier Mine, South Africa (Wagner 1914; Tolansky 1968). We now can explain these enigmatic diamonds by the absence of a free fluid phase in this kimberlite at the end of the emplacement. Our explanation agrees well with the rare geological features of Premier kimberlite attributed to "…insufficient volatile exsolution" (Skinner and Marsh 2004).

Given our experimental observations, the amount of resorption experienced by the diamonds can be used to infer the time at which a free fluid phase existed in a kimberlite system. As an example using our experimental data, the time required to produce a hexoctahedron from a 1 cm octahedron diamond at the NNO buffer is three days at 1350 °C and 0.5 days at 1500 °C. For a 0.5 cm diameter diamond, this time is 35 and 4 h, respectively (Fig. 9). In comparison to the rapid emplacement rates of kimberlite magmas—hours and days (Canil and Fedortchouk 1999; Kelley and Wartho 2000), these times suggest that to produce the resorbed diamonds found in the majority of kimberlites, a fluid phase should be present throughout a significant part of their emplacement history. Otherwise, the majority of the resorption could only have happened in the mantle source. The occurrence of pseudohemimorphic diamonds supports the large degree of resorption in kimberlites. These diamonds are partially protected by the enclosing mantle xenoliths and have only one side exposed to interaction with the kimberlite magma. Surface graphitization removed by later resorption could not produce such a high degree of diamond oxidation due to the much slower kinetics of this process.

Our experiments showed similar diamond oxidation rates in H_2O and in CO_2 fluids at the conditions of kimberlite magma during its ascent (Fig. 4a). However, the experiments at 100 kPa and 870 °C by Rudenko et al. (1979) produced a five-fold difference in diamond weight loss between oxidation in pure CO_2 and pure H_2O vapor. Very slow kinetics of diamond oxidation at these low temperature, however, suggest that the effect of the fluid composition on the diamond oxidation rate under near-surface conditions is insignificant.

Our experiments clearly show that resorption in H_2O and in CO_2 fluids produced very different surface features (Table 6). The majority of diamonds in the Panda, Beartooth, Misery kimberlites, and Lac de Gras field (Fedortchouk et al. 2005) show well-formed individual trigon etch pits, striations on the resorbed edges along the octahedron faces and on the surface of hexoctahedrons. Hillocks are common, but they have a round pyramid shape, similar to those produced in our experiments with H_2O. All these features indicate that at the last stages of kimberlite emplacement, the fluid that reacted with the diamonds from these pipes was mostly H_2O with and H_2O/CO_2 ratio much higher than those of proposed for the primary kimberlite melts of Wesselton (Shee 1986) and Jericho (Price et al. 2000).

In our experiments, we observed that diamond surface features record only the composition of the last fluid with which they reacted. Therefore, at this point we cannot tell much about the composition of the fluid in the kimberlites earlier history and evolution. A detailed study of the evolution of diamond surface features at variable fluid compositions compared to the features of different diamond groups within one population may shed more light on the evolution of kimberlitic fluid through the time. The observed relationship between the surface features of diamonds and composition of the fluid can provide a new tool to study the fluid system of kimberlites and, possibly, of the mantle source for diamonds.

ACKNOWLEDGMENTS

We thank Jon Carlson, Darren Dyck, and BHP Billiton Diamonds Inc. for providing us the diamonds for our experiments. Branko Deljanin and European Gemological Laboratories, Vancouver are thanked for help with collecting FTIR spectra and Patrick Hayman for the help with deconvolution of the spectra. We thank Valentin Afanasiev for valuable suggestions on the diamond resorption experiments and Stephen Parman on the experimental procedure. Bruce Kaye and Defence

Research and Development Canada are thanked for the help with obtaining Back Scatter Electron Images. Mati Raudsepp helped with MP analyses at UBC. We thank M. Arima and J. Jaszczak for constructive reviews. This research was supported by NSERC graduate scholarship to Y.F. and NSERC Discovery Grant to D.C.

REFERENCES CITED

Afanasiev, V.P., Yefimova, E.S., Zinchuk, N.N., and Koptil, V.I. (2000) Atlas of morphology of diamonds from Russian sources, 293 p. SPC UIGGM, Russian Academy of Science, Siberian Branch.

Arima, M. (1998) Experimental study of growth and resorption of diamond in kimberlitic melts at high pressures and temperatures. 7th International Kimberlite Conference, Extended Abstracts, p. 32–34, Cape Town.

Arima, M. and Kozai, Y. (2006) Growth and resorption of diamond by redox reactions in kimberlitic and carbonatitic melts. 19th International Mineralogical Association, Program and Abstract, 138, Kobe, Japan.

Brearley, M. and Scarfe, C.M. (1986) Dissolution rates of upper mantle minerals in an alkali basalt melt at high pressure: an experimental study and implications for ultramafic xenolith survival. Journal of Petrology, 27, 1157–1182.

Canil, D. and Fedortchouk, Y. (1999) Garnet dissolution and the emplacement of kimberlites. Earth and Planetary Science Letters, 167, 227–237.

——— (2001) Olivine-liquid partitioning of vanadium and other trace elements, with applications to modern and ancient picrites. The Canadian Mineralogist, 39, 319–330.

Chepurov, A.I., Khokhryakov, A.F., Sonin, V.M., and Pal'yanov, Y.N. (1985) Forms of dissolution of diamond crystals in silicate melts at high pressure. Doklady Academii Nauk SSSR, 285(1), 212–216 (in Russian).

Cull, F.A. and Meyer, H.O.A. (1986) Oxidation of diamond at high temperature and 1 atm total pressure with controlled oxygen fugacity. 4th International Kimberlite Conference, p. 377–379. Geological Society of Australia, Perth, Australia.

Davies, G. and Evans, T. (1972) Graphitization of diamond at zero pressure and at a high pressure. Proceedings of the Royal Society of London, Series A, Mathematical and Physical Sciences, 328(1574), 413–427.

Eggler, D.H. and Burnham, C.W. (1984) Solution of H_2O in diopside melts: a thermodynamic model. Contributions to Mineralogy and Petrology, 83, 58–66.

Evans, T. and Phaal, C. (1961) The kinetics of the diamond–oxygen reaction. Conference on Carbon, 5 PT.1, p. 147–153. Pergamon Press, New York.

Fedortchouk, Y., Canil, D., and Carlson, J.A. (2005) Dissolution forms in Lac de Gras diamonds and their relationship to the temperature and redox state of kimberlite magma. Contributions to Mineralogy and Petrology, 150, 54–69.

Gurney, J.J., Hildebrand, P.R., Carlson, J.A., Fedortchouk, Y., and Dyck, D.R. (2004) The morphological characteristics of diamonds from the Ekati property, Northwest Territories, Canada. Lithos, 77, 21–38.

Hayman, P.C., Kopylova, M.G., and Kaminsky, F.V. (2005) Lower mantle diamonds from Rio Soriso (Juina area, Mato Grosso, Brazil). Contributions to Mineralogy and Petrology, 149, 430–445.

Hays, J.F. (1966a) Lime-Alumina-Silica. Carnegie Institution Yearbook, 65, 234–239.

——— (1966b) Stability and properties of the synthetic pyroxene $CaAl_2SiO_6$. American Mineralogist, 51, 1524–1529.

Holloway, J.R. and Blank, J.G. (1994) Application of Experimental Results to C-O-H Species in Natural Melts. In M.R. Carrol, and J.R. Holloway, Eds. Volatiles in Magmas, 30, p. 187–230. Mineralogical Society of America, Chantilly, Virginia.

Kelley, S.P. and Wartho, J.-A. (2000) Rapid kimberlite ascent and the significance of Ar-Ar ages in xenolith phlogopites. Science, 289, 609–611.

Keppler, H. (2003) Water solubility in carbonatite melts. American Mineralogist, 88, 1822–1824.

Kozai, Y. and Arima, M. (2003) Diamond dissolution in kimberlite and lamproite melts at deep crustal conditions. Abstracts of 8th International Kimberlite Conference.

——— (2005) Experimental study on diamond dissolution in kimberliteic and lamproitic melts at 1300–1420 C and 1 GPa with controlled oxygen partial pressure. American Mineralogist, 90, 1759–1766.

McDade, P., Wood, B.J., VanWestrenen, W., Brooker, R., Gudmundsson, G., Soulard, H., Najorka, J., and Blundy, J. (2002) Pressure corrections for a selection of piston-cylinder cell assemblies. Mineralogical Magazine, 66, 1021–1028.

Mendelssohn, M.J. and Milledge, H.J. (1995) Morphological Characteristics of Diamond Populations in relation to Temperature-Dependent Growth and Dissolution Rates. International Geology Review, 37, 285–312.

Mitchell, R.H. (1986) Kimberlites: Mineralogy, geochemistry, and petrology, 464 p. Plenum Press, New York.

Pal'yanov, Y.N., Khokhryakov, A.F., Borzdov, Y.M., and Sokol, A.G. (1995) Diamond morphology in growth and dissolution processes. Extended Abstracts, 6th International Kimberlite Conference, 415–417.

Pouchou, J.L. and Pichoir, F. (1985) PAP φ(ρZ) procedure for improved quantitative microanalysis. Microbeam Analysis, 104–106.

Price, S.E., Russell, J.K., and Kopylova, M.G. (2000) Primitive magma from the Jericho pipe, NWT, Canada: constraints on primary kimberlite melt chemistry. Journal of Petrology, 41, 789–808.

Robinson, D.N., Scott, J.A., Neikerk, A.V., and Anderson, V.G. (1989) The sequence of events reflected in the diamonds of some southern African kimberlites. Kimberlites and related rocks, 2, no. 14, p. 990–1000.

Rudenko, A.P., Kulakova, I.I., and Shturman, V.L. (1979) Oxidation of natural diamond. Novye dannye o mineralogii SSSR, p. 105–125. Academiya Nauk SSSR, Fersman Mineralogical Museum, Moscow. (in Russian)

Shee, S.R. (1986) The petrogenesis of the Wesselton mine kimberlites, Kimberley, South Africa. University of Cape Town, Cape Town.

Skinner, E.M.W., and Marsh, J.S (2004) Distinct kimberlite pipe classes with contrasting eruption processes. Lithos, 76, 183–200.

Sonin, V.M., Zhimulev, Y.I., and Afanas'ev, V.P. (1997) Surface graphitization effect on diamond crystal morphology. Otechestvennaya Geologiya, 10, 33–37. (in Russian)

Sonin, V.M., Fedorov, I.I., Pokhilenko, L.N., and Pokhilenko, N.P. (2000) Diamond oxidation rate as related to oxygen fugacity. Geology of Ore Deposits, 42, 496–502.

Sonin, V.M., Zhimulev, E.I., Afanas'ev, V.P., and Chepurov, A.I. (2002) Genetic aspects of the diamond morphology. Geology of Ore Deposits, 44, 291–299.

Tolansky, S. (1968) Graphitized natural diamond. Diamond research, 8–10.

Wagner, P.A. (1914) Note on graphite-coated diamonds from the Premier Mine. Transactions of the Geological Society of South Africa, 17, 29–30.

Watson, E.B. (1987) Diffusion and solubility of C in Pt. American Mineralogist, 72, 487–490.

Watson, E.B., Wark, D.A., Price, J.D., and Van Orman, J.A. (2002) Mapping the thermal structure of solid-media pressure assemblies. Contributions to Mineralogy and Petrology, 142, 640–652.

Yamaoka, S., Kanda, H., and Setaka, N. (1980) Etching of diamond octahedrons at high temperatures and pressures with controlled oxygen partial pressure. Journal of Material Sciences, 15, 332–336.

Zhimulev, E.I., Sonin, V.M., and Chepurov, A.I. (2002) Formation of diamond crystals with faces protruding due to etching. Zapiski Vserossiyskogo Mineralogicheskogo Obshestva, 131, 111–113 (in Russian).

MANUSCRIPT RECEIVED AUGUST 12, 2006
MANUSCRIPT ACCEPTED MARCH 2, 2007
MANUSCRIPT HANDLED BY JOSHUA FEINBERG